



NOAA Technical Memorandum, OAR AOML-98

**PROCEDURES TO CREATE NEAR REAL-TIME SEASONAL AIR-SEA
CO₂ FLUX MAPS**

G. Park
R. Wanninkhof
J. Triñanes

Atlantic Oceanographic and Meteorological Laboratory
Miami, Florida

February 2010

noaa

**NATIONAL OCEANIC AND
ATMOSPHERIC ADMINISTRATION**

**Office of Oceanic and
Atmospheric Research**

**PROCEDURES TO CREATE NEAR REAL-TIME SEASONAL AIR-SEA
CO₂ FLUX MAPS**

Geun-Ha Park¹
Rik Wanninkhof²
Joaquin A. Triñanes³

¹University of Miami/Cooperative Institute for Marine and Atmospheric Studies
Miami, Florida

²NOAA/Atlantic Oceanographic and Meteorological Laboratory
Miami, Florida

³University of Santiago de Compostela/Technological Research Institute
Santiago de Compostela, Spain

February 2010



**UNITED STATES
DEPARTMENT OF COMMERCE**

**Mr. Gary Locke
Secretary**

**NATIONAL OCEANIC AND
ATMOSPHERIC ADMINISTRATION**

**Dr. Jane Lubchenco
Undersecretary for Oceans and
Atmosphere/Administrator**

**Office of Oceanic and
Atmospheric Research**

**Dr. Richard W. Spinrad
Assistant Administrator**

Disclaimer

NOAA does not approve, recommend, or endorse any proprietary product or material mentioned in this document. No reference shall be made to NOAA or to this document in any advertising or sales promotion which would indicate or imply that NOAA approves, recommends, or endorses any proprietary product or proprietary material herein or which has as its purpose any intent to cause directly or indirectly the advertised product to be used or purchased because of this document.

The findings and conclusions in this report are those of the authors and do not necessarily represent the views of the funding agency.

Table of Contents

List of Figures.....	iv
List of Acronyms.....	v
Abstract.....	1
1. Introduction.....	1
2. Calculation Method.....	2
2.1 Global $\Delta p\text{CO}_2$ Climatology.....	3
2.2 Subannual Relationships between $p\text{CO}_{2\text{SW}}$ and SST, $(\partial p\text{CO}_{2\text{SW}}/\partial \text{SST})_{2000\text{m}}$	3
2.3 Sea Surface Temperature.....	6
2.4 Wind Speed.....	7
2.5 Sea-Ice Cover.....	7
3. Results and Discussion.....	8
3.1 Overall Magnitude of Anomalies.....	8
3.2 Regional Changes.....	9
3.3 Seasonal Changes.....	10
4. Caveats.....	11
5. The Near Real-Time CO_2 Flux Product.....	11
6. Conclusions.....	11
7. Acknowledgments.....	12
8. References.....	13

List of Figures

Figure 1.	A select comparison of three fixed seasonal and optimum subannual $p\text{CO}_{2\text{SW}}$ -SST relationships.....	4
Figure 2.	A select comparison of air-sea CO_2 flux values estimated from three fixed seasonal and optimum subannual $p\text{CO}_{2\text{SW}}$ -SST relationships in pixels centered on 40°S , 52.5°E and 48°N , 152.5°E	6
Figure 3.	Net global air-sea CO_2 fluxes in Pg C yr^{-1} for 1982-2007 and CO_2 efflux anomalies relative to the 26-year mean value for the Equatorial Pacific	8
Figure 4.	Climatological air-sea CO_2 flux map from Takahashi <i>et al.</i> (2009) and magnitude of interannual air-sea CO_2 flux variability in each pixel for 26 years.....	9
Figure 5.	Interannual variability (1σ) of the net air-sea CO_2 flux in each pixel for four seasons	10
Figure 6.	Interface from the website that enables the retrieval of graphic and numeric data for the empirical air-sea CO_2 flux product discussed in this study.....	12

List of Acronyms

AOML	Atlantic Oceanographic and Meteorological Laboratory
CO ₂	Carbon dioxide
DIC	Dissolved inorganic carbon
DOE	Department of Energy
ENSO	El Niño-Southern Oscillation
ESRL	Earth System Research Laboratory
NCEP	National Centers for Environmental Prediction
NOAA	National Oceanic and Atmospheric Administration
OI	Optimum interpolation
pCO ₂	Partial pressure of carbon dioxide
pCO _{2AIR}	Partial pressure of carbon dioxide in atmosphere
pCO _{2SW}	Partial pressure of carbon dioxide in surface seawater
SOOP	Ship of opportunity
SSS	Sea surface salinity
SST	Sea surface temperature
TA	Total alkalinity

Procedures to Create Near Real-Time Seasonal Air-Sea CO₂ Flux Maps

Abstract

Seasonal air-sea carbon dioxide (CO₂) flux maps were calculated from wind speed data and the difference in CO₂ partial pressure between surface seawater (pCO_{2SW}) and the overlying atmosphere. To infer the seasonal variability of global net air-sea CO₂ fluxes over the last three decades, we derived the optimum subannual relationships between pCO_{2SW} and the sea surface temperature (SST). These optimum subannual relationships accounted for the variations between pCO_{2SW} and SST and showed significantly better correlations than previous relationships with fixed monthly boundaries. The derived algorithms were then applied to high-resolution SST data to yield changes in pCO_{2SW} on a monthly basis. The pCO_{2SW} values were also combined with a gas transfer velocity estimate derived from high resolution wind products to estimate seasonal fluxes. The seasonal fluxes that are calculated with a three- to six-month lag from real-time can be obtained at <http://cwcgom.aoml.noaa.gov/erddap/griddap/aomlcarbonfluxes.graph>. Here, we describe in detail the procedures and uncertainties of this product.

1. Introduction

The ocean is an important sink for atmospheric CO₂, absorbing 20-30% of the annual release of anthropogenic CO₂ (Sabine *et al.*, 2004). However, oceanic CO₂ uptake is highly variable in time and space, and its interannual variability has not been well constrained. The global surface CO₂ database is currently too sparse, except for a few regions, to quantify the air-sea CO₂ flux variability on the required spatial and temporal scales, and other approaches need to be applied. The recent increase in CO₂ partial pressure (pCO₂) measurements from moorings and Ships of Opportunity (SOOP) now makes direct interpolation of these data possible for certain regions, particularly when auxiliary parameters such as SST and mixed layer depth, as well as advanced interpolation procedures such as self-organizing maps and multi-linear regression, are used (e.g., Telszewski *et al.*, 2009). The ultimate goal of NOAA's Climate Observation Division and Global Carbon Cycle Program is to establish a global observing network comprised of research ships, SOOP, and moorings that can resolve basin-wide fluxes of CO₂ on seasonal timescales to $\pm 0.2 \text{ Pg} (10^{15} \text{ g}) \text{ C}$.

In the interim, CO₂ seasonal fluxes can be estimated using the air-sea CO₂ flux climatology of Takahashi *et al.* (2009), along with high resolution wind and SST data using the procedures outlined below. The interannual variability of global net air-sea CO₂ flux is based on algorithms between pCO_{2SW} and SST. In this study, we assumed that the subannual pCO_{2SW}-SST relationships derived from the climatology for each pixel, along with interannual SST anomalies, accounted for the interannual variations in pCO_{2SW}. SST as a parameter has been available with global distribution over the past decade and can reasonably account for changes in pCO_{2SW} caused by thermodynamic, biological, and physical mixing effects.

2. Calculation Method

Changes in $p\text{CO}_{2\text{SW}}$ are controlled by variations of SST, sea surface salinity (SSS), dissolved inorganic carbon (DIC), and total alkalinity (TA). These changes can be expressed by the following deconvolution:

$$\partial p\text{CO}_{2\text{SW}} = \frac{\partial p\text{CO}_{2\text{SW}}}{\partial \text{SST}} \times \Delta \text{SST} + \frac{\partial p\text{CO}_{2\text{SW}}}{\partial \text{SSS}} \times \Delta \text{SSS} + \frac{\partial p\text{CO}_{2\text{SW}}}{\partial \text{DIC}} \times \Delta \text{DIC} + \frac{\partial p\text{CO}_{2\text{SW}}}{\partial \text{TA}} \times \Delta \text{TA} \quad (1)$$

where $\partial p\text{CO}_{2\text{SW}}$ is the change in $p\text{CO}_{2\text{SW}}$, $\partial p\text{CO}_{2\text{SW}}/\partial \text{XXX}$ are the partial derivatives with respect to the varying quantity ΔXXX , and XXX is either SST, SSS, DIC, or TA. Among these, SST is the most important factor affecting the change in $p\text{CO}_{2\text{SW}}$. The SST effect on $p\text{CO}_{2\text{SW}}$ under isochemical conditions ($\partial \ln p\text{CO}_{2\text{SW}}/\partial \text{SST}$) is $\approx 4.23\% \text{ C}^{-1}$ (Takahashi *et al.*, 1993). Changes in DIC and TA concentrations in the surface ocean are caused by deep-water upwelling (transport effect) and photosynthesis (biological effect). These changes are often accompanied by SST changes. SSS represents only a small proportion of the overall variability of the total $p\text{CO}_{2\text{SW}}$ (Takahashi *et al.*, 1980). Therefore, SST accounted either directly or indirectly for the thermodynamic, transport, and biological effects that cause changes in $p\text{CO}_{2\text{SW}}$. The decadal record of SST makes it a good parameter to account for the temporal variations in $p\text{CO}_{2\text{SW}}$.

The monthly net air-sea CO_2 fluxes (F_{ym}) for each 4° latitude \times 5° longitude pixel for individual years were calculated from the global $\Delta p\text{CO}_2$ climatology of Takahashi *et al.* (2009), monthly mean wind speed, and SST anomalies compared to SST data for the reference year 2000 in the following manner:

$$F_{ym} = k_{ym} K_{0,ym} \{ [p\text{CO}_{2\text{SW } 2000m} + (\partial p\text{CO}_{2\text{SW}}/\partial \text{SST})_{2000m} \times \Delta \text{SST}_{ym-2000m}] - p\text{CO}_{2\text{AIR } 2000m} \}, \quad (2)$$

where the subscript ym is the year and month in the time series during the study period, and the subscript $2000m$ refers to the month in 2000. The solubility of CO_2 , K_0 , was estimated from monthly SST and climatological SSS estimates using the solubility equations of Weiss (1974):

$$\begin{aligned} K_0 \text{ (mol/kg}\cdot\text{atm)} &= \exp(-60.2409 + 9345.17 / (\text{SST} + 273.15) + 23.3585 \times \\ &\ln((\text{SST} + 273.15) / 100) + \text{SSS} \times (0.023517 - 0.00023656 \times \\ &(\text{SST} + 273.15) + 0.00000047036 \times (\text{SST} + 273.15)^2)). \end{aligned} \quad (3)$$

The monthly gas transfer velocity, k_{ym} , was determined from the second moment of the monthly mean wind speed:

$$k_{ym} = 0.217 \times \langle U_{10,ym}^2 \rangle (\text{Sc}_{ym}/660)^{-0.5}, \quad (4)$$

where $\langle U_{10,ym}^2 \rangle$ is the second moment representing the variance of the 6-hour wind speed in each pixel, and Sc is the Schmidt number calculated according to Wanninkhof (1992) using the monthly SST for each pixel. The coefficient 0.217 is the adjusted value from the coefficient 0.26

for the monthly wind speed normalized to a 10-m height above the surface (U_{10}) as used by Takahashi *et al.* (2009) with $\langle U_{10}^2 \rangle / \langle U_{10} \rangle^2$ of 1.2 ($0.26/1.2 = 0.217$). These coefficients are based on an improved assessment of the global ^{14}C inventory used to constrain the global gas transfer velocity (Sweeney *et al.*, 2007). In the polar regions where sea-ice forms seasonally, k_{ym} was multiplied by $(1-f)$, where f is the fractional sea-ice cover.

2.1 Global ΔpCO_2 Climatology

The monthly global ΔpCO_2 ($\text{pCO}_{2\text{SW}} - \text{pCO}_{2\text{AIR}}$) climatology of Takahashi *et al.* (2009) is for non-El Niño conditions. It was produced using approximately three million measurements of $\text{pCO}_{2\text{SW}}$ obtained from 1970 to 2007 by over 30 investigators. Atmospheric pCO_2 ($\text{pCO}_{2\text{AIR}}$) values (GLOBALVIEW-CO₂, 2008) are for the reference year 2000. The ΔpCO_2 climatology used in this study is available at www.ldeo.columbia.edu/res/pi/CO2/carbondioxide/pages/air_sea_flux_2009.html. All $\text{pCO}_{2\text{SW}}$ measurements were normalized to the reference year 2000 and interpolated to a 4° latitude \times 5° longitude spatial grid using a two-dimensional diffusion-advection transport model for surface waters. Even with three million data points on a $4^\circ \times 5^\circ$ grid, the surface ocean remains undersampled (see Figure 1 in Takahashi *et al.*, 2009). This database is about three times larger than the 0.94 million measurements used for the previous climatology (Takahashi *et al.*, 2002). Its observational density has been significantly increased and covers more geographic areas, particularly the subpolar Southern Ocean.

2.2 Subannual Relationships between $\text{pCO}_{2\text{SW}}$ and SST, $(\partial\text{pCO}_{2\text{SW}}/\partial\text{SST})_{2000\text{m}}$

For areas outside of the central and eastern Equatorial Pacific, optimum subannual $\text{pCO}_{2\text{SW}}$ -SST relationships for each $4^\circ \times 5^\circ$ pixel were derived from least squares linear fits of monthly climatological $\text{pCO}_{2\text{SW}}$ and SST values. Optimum subannual $\text{pCO}_{2\text{SW}}$ -SST relationships were made using at least three consecutive monthly values according to the monthly variation pattern of the two parameters for each pixel to avoid spurious values of $(\partial\text{pCO}_{2\text{SW}}/\partial\text{SST})_{2000\text{m}}$ that can arise by determining the trend from month to month. Therefore, each pixel had from one to four subannual relationship(s) between $\text{pCO}_{2\text{SW}}$ and SST, and the monthly range of subannual relationships for each pixel could be different (Figure 1).

We used the following criteria to optimize the subannual relationships of $\text{pCO}_{2\text{SW}}$ and SST values and to minimize the number of subannual relationships for each pixel. First, a linear fit equation was made from 12 months of data. If its correlation coefficient (R^2) was more than 0.9, one $\text{pCO}_{2\text{SW}}$ -SST relationship was accepted. If its correlation coefficient was below 0.9, we derived subannual relationships using at least three consecutive monthly values. Among them, we selected relationships in the following manner: (1) all correlation coefficients had to be greater than 0.5; (2) relationships with a higher mean value of the correlation coefficient were retained; (3) we strived for a minimum number of relationships and maximum number of months in each relationship (when relationships had similar correlation coefficients, this step (3) took precedence over step (2)). If a particular pixel's subannual relationships with all R^2 greater than 0.5 could not be found, we selected subannual boundaries with more relationships of R^2 greater than 0.5 and a higher mean value of R^2 .

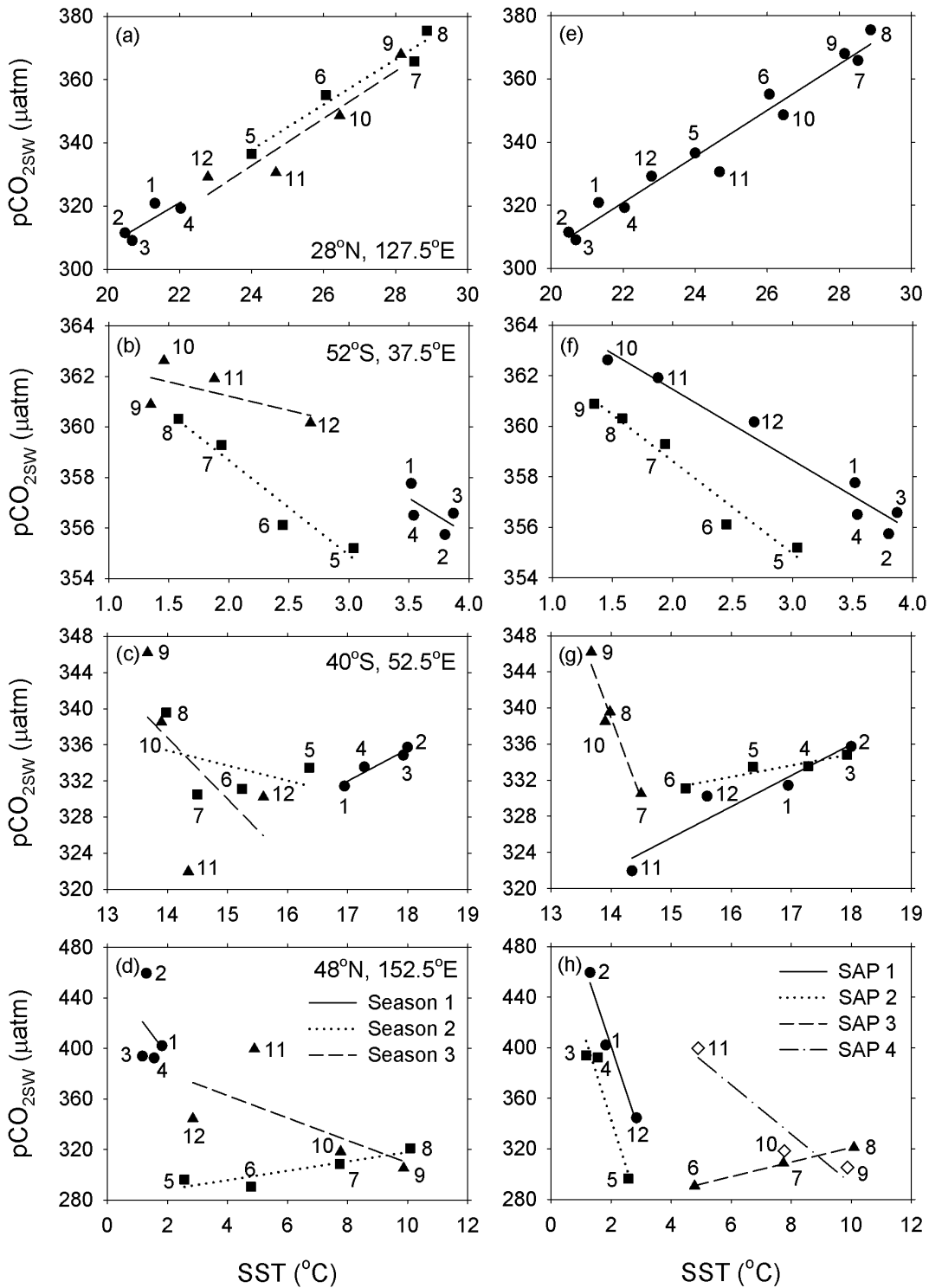


Figure 1. A select comparison of three fixed seasonal (a-d) and optimum subannual pCO_{2sw} -SST relationships (e-h). The numbers correspond to the month of the year. The solid circles and solid lines show season 1 for three fixed seasonal relationships and Subannual Period 1 (labeled with SAP 1) for optimum subannual relationships, solid squares and dotted lines are for season 2 and Subannual Period 2, solid triangles and dashed lines are for season 3 and Subannual Period 3, and the open diamonds and dash-dotted lines depict Subannual Period 4 for the subannual relationships. The center of each pixel is listed in figures a–d and corresponds to the same location for the graph immediately to its right.

This approach differs from the way ($\partial p\text{CO}_{2\text{SW}}/\partial \text{SST}$) has been determined in previous studies (Lee *et al.*, 1998; Park *et al.*, 2006) that used seasonal $p\text{CO}_{2\text{SW}}$ -SST relationships derived from monthly $p\text{CO}_{2\text{SW}}$ and SST values for three fixed time periods: January-April (season 1), May-August (season 2), and September-December (season 3). Low correlations between $p\text{CO}_{2\text{SW}}$ and SST were found in several regions and seasons in these studies, particularly in the Southern and South Indian oceans. Moreover, with three fixed seasonal relationships, many pixels with low correlation coefficients ($R^2 < 0.5$) were found in the high latitude oceans during the boreal winter season. For example, for season 1, 62% of the total number of pixels showed correlation coefficients lower than 0.5. This indicates that variations of $p\text{CO}_{2\text{SW}}$ were not well correlated with SST changes during the boreal winter season (season 1) with fixed monthly boundaries (Figures 1c and 1d). To determine the reason for the low correlations, we checked the variation patterns of $p\text{CO}_{2\text{SW}}$ and SST in detail. Most of the low correlations were due to the criteria of fixed monthly boundaries. If the trend between $p\text{CO}_{2\text{SW}}$ and SST variations changed within the fixed monthly boundary, we obtained a low correlation value of the relationship. When flexible monthly boundaries were applied to each pixel, only 1% of the total pixels showed weak correlations between SST and $p\text{CO}_{2\text{SW}}$. The mean correlation coefficient for all the pixels was 0.83 ± 0.14 . This good correlation indicates that SST changes can reasonably account for $p\text{CO}_{2\text{SW}}$ variability in most of the pixels.

Figure 1 shows the difference between the optimum subannual relationships and the previous approach of the three fixed seasonal relationships for select pixels. With the optimum subannual relationships, 18% of the total pixels, which are mainly distributed over northern subtropical regions, had one $p\text{CO}_{2\text{SW}}$ -SST relationship, and 24% of the total pixels had two subannual relationships. Half of the total pixels had three subannual relationships; however, only 20% of them had the same monthly ranges as the three fixed seasonal relationships. Seven percent of the pixels had four subannual $p\text{CO}_{2\text{SW}}$ -SST relationships. At high latitudes, a few pixels (<10) showed no meaningful subannual $p\text{CO}_{2\text{SW}}$ -SST relationships because there were no significant temporal variations of the climatological $p\text{CO}_{2\text{SW}}$ or SST.

Examples of the effect of change in subannual relationships on the yearly air-sea CO_2 flux values are shown in Figure 2. The larger changes and the greater increases of interannual variability in CO_2 fluxes were found in the pixels that had low correlation coefficients of relationships within the fixed monthly boundaries and the larger SST variations (Figure 2b). However, the interannual variabilities of global air-sea CO_2 flux values estimated from the three fixed seasonal and optimum subannual relationships were the same ($0.13 \text{ Pg C (} 10^{15} \text{ g C) yr}^{-1}$, respectively). These similarities were due to a cancellation of positive and negative fluxes in pixels and damping of the interannual signal when the fluxes were summed over the global scale.

For the central and eastern Equatorial Pacific (6°N - 10°S and 80°W - 165°E), we used updated empirical $p\text{CO}_{2\text{SW}}$ -SST equations derived from multiyear data that were collected in the Equatorial Pacific between 1981 and 2004 (Feely *et al.*, 2006). It is well known that the drivers of interannual variability in this region are different from those of seasonal variability, invalidating our basic assumptions. Moreover, this is one of the regions with a sufficient amount of $p\text{CO}_{2\text{SW}}$ data gathered over the past 30 years that enabled us to interpolate the data to discern their interannual variability (Feely *et al.*, 2006) rather than rely on our empirical approach. Because this dataset covers all phases of El Niño and La Niña periods for the past three decades, these $p\text{CO}_{2\text{SW}}$ -SST equations could account for $p\text{CO}_{2\text{SW}}$ changes caused by the El Niño-Southern

Oscillation (ENSO) better than seasonal relationships derived from the monthly climatology based on non-El Niño conditions. Twelve $p\text{CO}_{2\text{SW}}\text{-SST}$ equations representing the warm (January to June) and cool (July to December) seasons of both El Niño and non-El Niño conditions for three time periods (1979-1989, 1990-1997, and 1998-2004) were used in this study (see Table 3 in Feely *et al.*, 2006). El Niño and non-El Niño periods are based on SST anomalies in the Niño 3.4 region ($5^{\circ}\text{N}\text{-}5^{\circ}\text{S}$ and $120^{\circ}\text{W}\text{-}170^{\circ}\text{W}$) (Trenberth, 1997). The $p\text{CO}_{2\text{SW}}$ values after 2004 were calculated from the equations for the period 1998-2004. To estimate a net air-sea CO_2 flux in the central and eastern Equatorial Pacific, mean $p\text{CO}_{2\text{AIR}}$ values for the three time periods were calculated from mole fractions of CO_2 obtained from the National Oceanic and Atmospheric Administration's Earth System Research Laboratory (NOAA-ESRL) (GLOBALVIEW- CO_2 , 2008).

2.3 Sea Surface Temperature

The monthly mean SST data used in this work were from NOAA's Optimum Interpolation (OI) SST V2 data processed from 1982 onward (available at www.cdc.noaa.gov/data/gridded/data.noaa.oisst.v2.html). These smoothed assimilated data are a blend of in-situ and satellite SSTs and are available on a 1° latitude \times 1° longitude grid. The original monthly data were re-gridded onto a $4^{\circ} \times 5^{\circ}$ grid to match the grid size of the $\Delta p\text{CO}_2$ climatology.

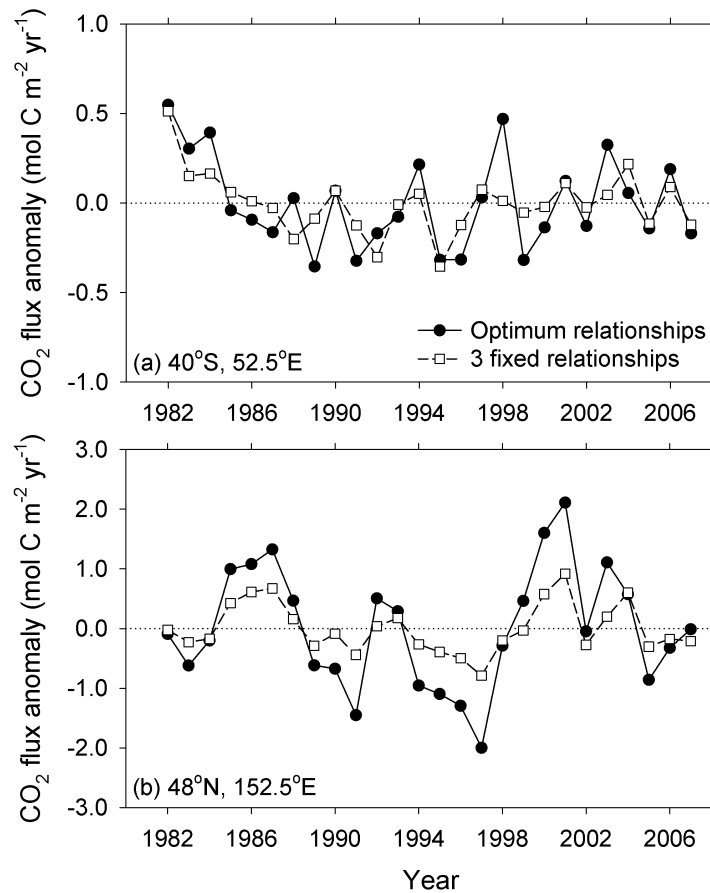


Figure 2. A select comparison of air-sea CO_2 flux values estimated from three fixed seasonal and optimum subannual $p\text{CO}_{2\text{SW}}\text{-SST}$ relationships in pixels centered on $40^{\circ}\text{S}, 52.5^{\circ}\text{E}$ (a) and $48^{\circ}\text{N}, 152.5^{\circ}\text{E}$ (b). The corresponding $p\text{CO}_{2\text{SW}}\text{-SST}$ relationships are shown in Figures 1c, 1d, 1g, and 1h, respectively.

NOAA's OI SST V2 database is the second version of the OI SST product recomputed for late 1981 onward using consistent methods. The most significant change for the OI SST V2 data is a reduction of biases in the OI SST at higher latitudes due to an improved simulation technique that uses sea-ice data. Improved ship data coverage used in the update and extension of the Comprehensive Ocean-Atmosphere Data Set (COADS) has also reduced the satellite SST biases in otherwise data-sparse regions (Reynolds *et al.*, 2002).

2.4 Wind Speed

The monthly mean wind speed data used in this study were acquired from the 6-hour (four times a day) data of the National Centers for Environmental Prediction-Department of Energy (NCEP-DOE) reanalysis 2 product plotted on a Gaussian grid¹ (available at www.cdc.noaa.gov/data/gridded/data.ncep.reanalysis2.html). The statistical analysis uses all wind data within each $4^\circ \times 5^\circ$ pixel, properly masked for land. The land mask for computing the $4^\circ \times 5^\circ$ monthly wind fields is from NOAA's OI SST V2 product.

The NCEP-DOE reanalysis product was created to produce a 40-year record of global atmospheric fields of research quality data suitable for many uses including weather and climate applications. This reanalysis 2 product is an improved version of the original NCEP reanalysis product in that it fixed errors and updated parameterizations of physical processes (Kanamitsu *et al.*, 2002).

Wind speed directly controls the magnitude of the air-sea CO₂ flux for a given $\Delta p\text{CO}_2$ (see eqn. 2). The higher wind speeds yield higher air-sea CO₂ fluxes. Therefore, wind speed variability is an important factor for quantifying changes in the air-sea CO₂ flux. The NCEP wind speed product contains significant different values and temporal trends at high latitudes when compared with satellite-based wind speed data (Wallcraft *et al.*, 2009). However, the degree of bias and its effect on the variability of the air-sea CO₂ fluxes has not yet been fully resolved.

2.5 Sea-Ice Cover

At high latitudes, ice cover has a significant effect on the air-sea CO₂ flux. In winter, sea-ice covering the surface ocean inhibits CO₂ gas exchange at the air-sea interface. In summer, sea-ice melts and the air-sea CO₂ exchange resumes. Moreover, pCO_{2SW} levels near the ice edge show large seasonal changes with large minima in the spring due to high biological productivity and high values in the fall and winter due to vertical advection and mixed layer deepening.

The monthly fractional sea-ice cover values (f) were obtained from the monthly NOAA OI SST V2 surface ice concentration fields (available at www.cdc.noaa.gov/data/gridded/data.noaa.oisst.v2.html). The original data were plotted on a 1° latitude \times 1° longitude grid for the

¹A Gaussian grid is used in the earth sciences as a grid for scientific modeling on a sphere. It can be uniquely accessed by one-dimensional latitude and longitude arrays (orthogonal coordinates). The longitudes are equally spaced, while the latitudes are unequally spaced according to the Gaussian quadrature. Gaussian grids do not have points at the poles, and the grid cells typically have an aspect ratio of longitude to latitude of 1:2. There are different Gaussian grids for different models and data providers. The NCEP-DOE reanalysis 2 product uses the global T2 Gaussian grid with 192×94 points.

study period and were re-gridded to a $4^\circ \times 5^\circ$ grid. When the ice cover value was less than 0.1, each pixel was regarded as a sea-ice-free area. When the ice cover value was greater than 0.9, we assumed that each pixel had 10% ice-free open water ($f = 0.9$) because air-sea CO_2 fluxes can be enhanced by leads caused by dynamic motions of sea-ice (Takahashi *et al.*, 2009).

3. Results and Discussion

3.1 Overall Magnitude of Anomalies

Our empirical model obtained a 26-year global mean net air-sea CO_2 flux of $1.49 \text{ Pg C yr}^{-1}$ for the period 1982-2007 (Figure 3a). The global net air-sea CO_2 fluxes showed a strong correlation with the ENSO cycle, which confirms that large-scale climate reorganizations have a key effect on the interannual variability of air-sea CO_2 fluxes. Higher oceanic CO_2 uptakes have occurred during El Niño periods that are mainly due to relatively low CO_2 efflux in the Equatorial Pacific (Figures 3a and 3b). Our analysis showed that the interannual variability of the global net air-sea CO_2 flux was $\pm 0.13 \text{ Pg C yr}^{-1}$ (1σ) for the period 1982-2007.

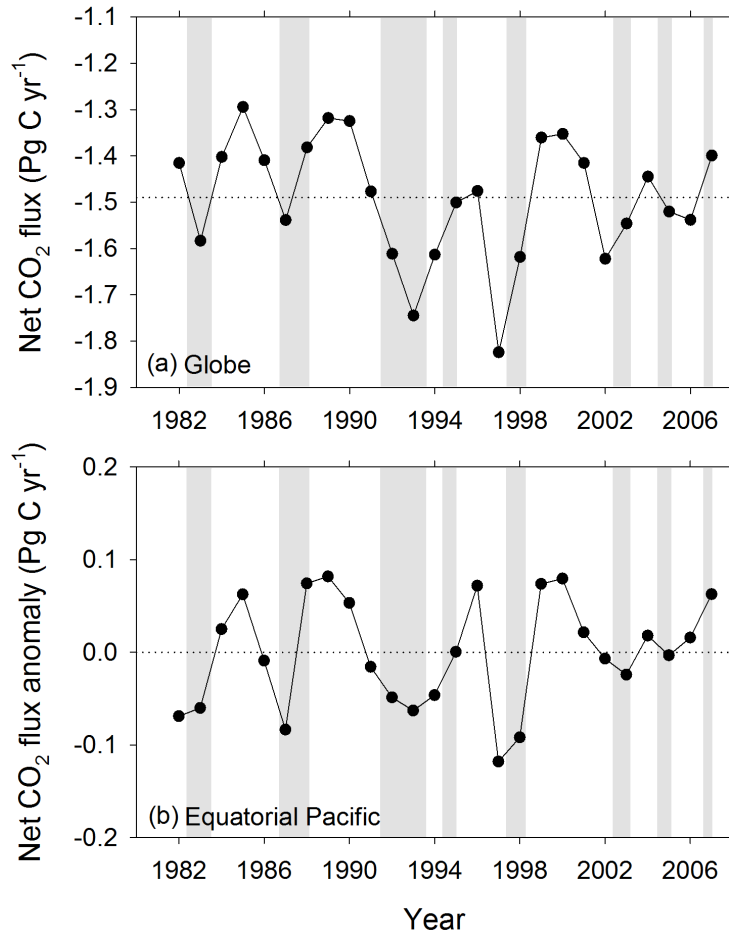


Figure 3. (a) Net global air-sea CO_2 fluxes in Pg C yr^{-1} for 1982-2007. Negative values denote net oceanic CO_2 uptake. Shaded bars indicate El Niño periods (based on SST changes in the Niño 3.4 region). The dotted line denotes a 26-year global mean air-sea CO_2 flux. (b) CO_2 efflux anomalies relative to the 26-year mean value for the Equatorial Pacific (10°N - 10°S , 80°W - 135°E).

3.2 Regional Changes

Large interannual variabilities were found in the high latitude North Atlantic, Equatorial Pacific, Southern Ocean, and mid North Pacific which correspond to the CO₂ sink and source regions on the global net air-sea CO₂ flux map (Figures 4a and 4b). The high latitude North Atlantic (north of 50°N, Figure 4a), the most intense CO₂ uptake area, had a large interannual variability due mainly to large changes in SST anomalies and the steep seasonal relationships between pCO_{2SW} and SST. The Equatorial Pacific, the most permanent CO₂ source area, showed large interannual variability closely connected with the ENSO cycle that determines the intensity of the upwelling of deep waters rich in CO₂ (Figures 3b and 4). Although a seasonal upwelling of deep water occurs in the Indian Ocean due to the Southwest Monsoon winds, the Indian Ocean had relatively low interannual variability when compared to the other two major oceans.

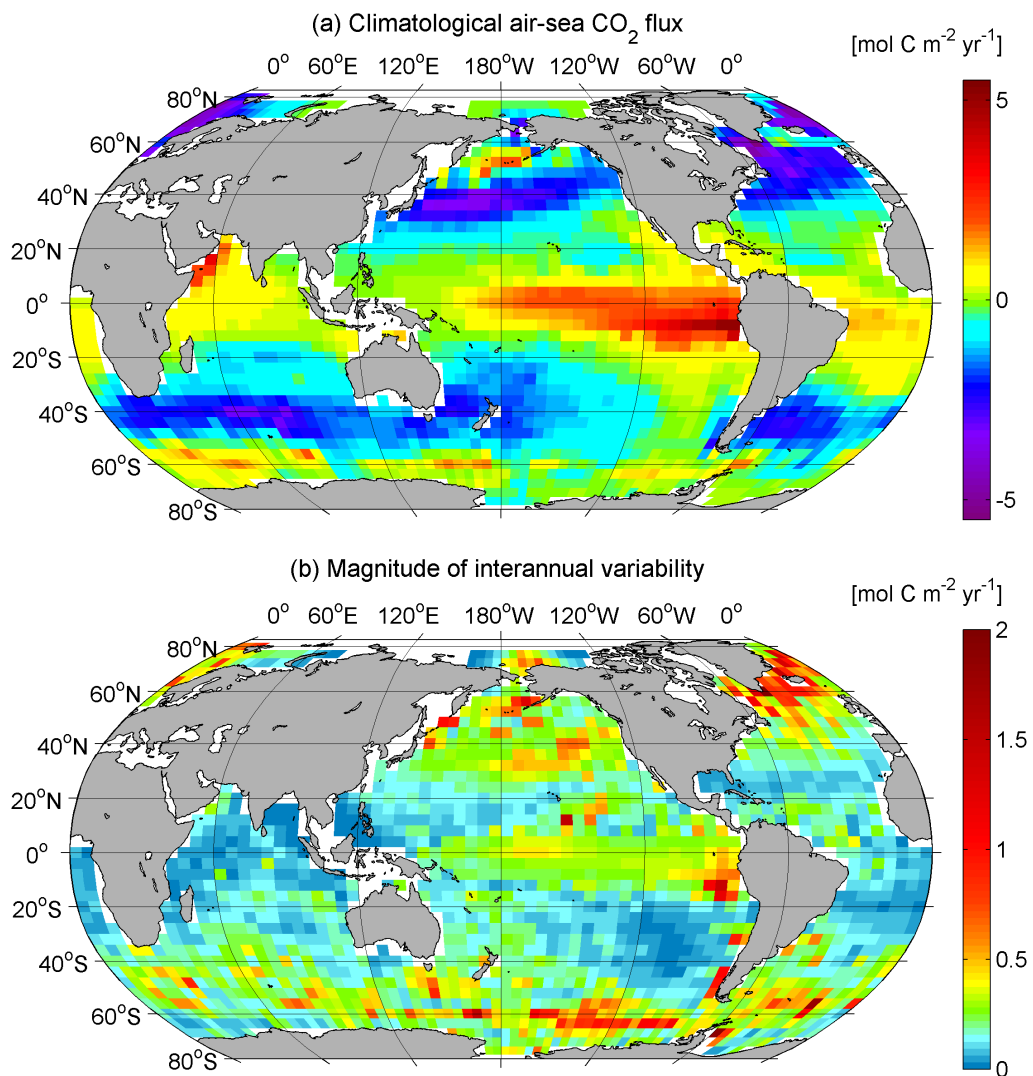


Figure 4. (a) Climatological air-sea CO₂ flux map from Takahashi *et al.* (2009) and (b) magnitude of interannual air-sea CO₂ flux variability in each pixel for 26 years. The magnitude of interannual variability is expressed as a standard deviation (1σ) from the 26-year annual mean of net air-sea CO₂ fluxes in each pixel.

The yearly net air-sea CO₂ flux in the Southern Ocean is controlled by the net difference between a significant drawdown of surface pCO_{2SW} by biological production in summer and the upwelling of CO₂-rich deep waters in winter. The pCO_{2SW} change in this region is 180 degrees out of phase with SST, and its seasonal magnitude is as great as 100 μatm. This allowed for negative seasonal pCO_{2SW}-SST relationships (with high sensitivity for SST anomalies), leading to high interannual variability in the air-sea CO₂ flux.

3.3 Seasonal Changes

Figure 5 shows the interannual air-sea CO₂ flux anomalies from four seasons for the 26-year mean seasonal CO₂ flux values based on the total interannual variability of each pixel. Each season has a range of three months: December-February, March-May, June-August, and September-November. The North Pacific and North Atlantic oceans showed large interannual variabilities in the boreal winter and spring seasons (Figures 5a and 5b) and small variabilities in the summer (Figure 5c). The El Niño phenomenon that mainly controls surface pCO_{2SW} in the Equatorial Pacific typically persists from late fall to the following spring. The efflux in the Equatorial Pacific showed large interannual changes in that season (Figure 5a). In the Southern Ocean, large variabilities were found near the ice edge in all of the seasons except austral summer (Figures 5b, 5c, and 5d).

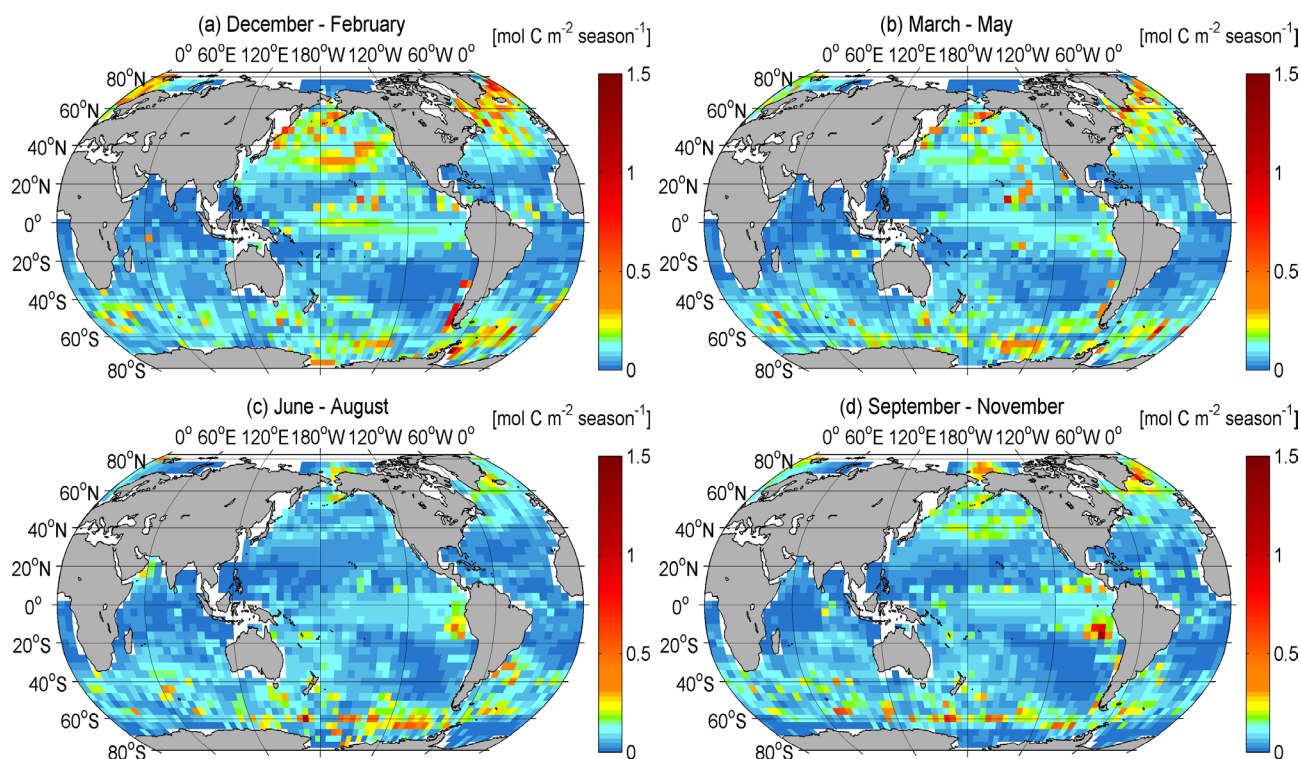


Figure 5. Interannual variability (1σ) of the net air-sea CO₂ flux in each pixel for the four seasons of (a) December-February, (b) March-May, (c) June-August, and (d) September-November for 26 years.

4. Caveats

While we believe, based on a comparison with models and time series stations, that the approach outlined in this study faithfully reproduces the interannual variability of air-sea CO₂ fluxes, there are some caveats that could lead to an underestimation of the variability. The most important caveat is that this method is unable to detect changes that are not correlated with temperature. We also implicitly assumed that for all regions/pixels, except the eastern and central Equatorial Pacific, that the subannual trends in SST and pCO_{2SW} could be used to determine interannual variations. For large-scale climate reorganizations such as the North Atlantic Oscillation and the Southern Annular Mode, there are other possible trends that are not captured with this approach. Finally, the approach assumed that there is no long-term trend in ΔpCO₂ other than changes that correspond to long-term SST trends (see eqn 1). We, therefore, believe that while interannual variability is well represented by this approach, decadal trends in the fluxes are not adequately captured.

5. The Near Real-Time CO₂ Flux Product

The release of pCO_{2SW} data generally does not occur within two years of their acquisition due to the time it takes to quality control the data, agreements on when the data can be released, and the ad-hoc arrangements to collate and release uniform/global datasets. Since global SST and wind data can be obtained within months of their collection, our approach provides a powerful means to determine month-to-month changes in near real-time. The near real-time flux maps can be obtained at <http://cwcgom.aoml.noaa.gov/erddap/griddap/aomlcarbonfluxes.graph>. A graphical user interface allows a user to select regional and global monthly maps from 1982 onward, and data can be exported in a variety of graphic and numeric formats. Moreover, time series plots can be created for any particular pixel. A screen shot of the web-based interface is presented in Figure 6.

6. Conclusions

An improved understanding of the year-to-year variations in CO₂ uptake is necessary to predict the future response of the carbon cycle to climate change. To accomplish this, the regions and processes that control the interannual variations of the ocean and land biosphere must be determined. Here, we modeled interannual variability in the net air-sea CO₂ fluxes using an updated subannual pCO_{2SW}-SST algorithms. These improved subannual algorithms, along with improved SST and wind speed data sets, allowed us to produce more reliable air-sea CO₂ flux maps than previous endeavors. These near real-time air-sea CO₂ flux maps can be obtained from the above mentioned website and are useful in detecting basin-wide variations of net air-sea CO₂ fluxes on seasonal scales and improve our understanding of the carbon cycle. This material serves an important outreach function for the public and other groups by enabling them to become better informed about NOAA's ocean carbon research efforts. With the ongoing collection of SOOP, mooring, and satellite data, we will be able to resolve temporal variations of air-sea CO₂ fluxes with more confidence and higher accuracy in the future.

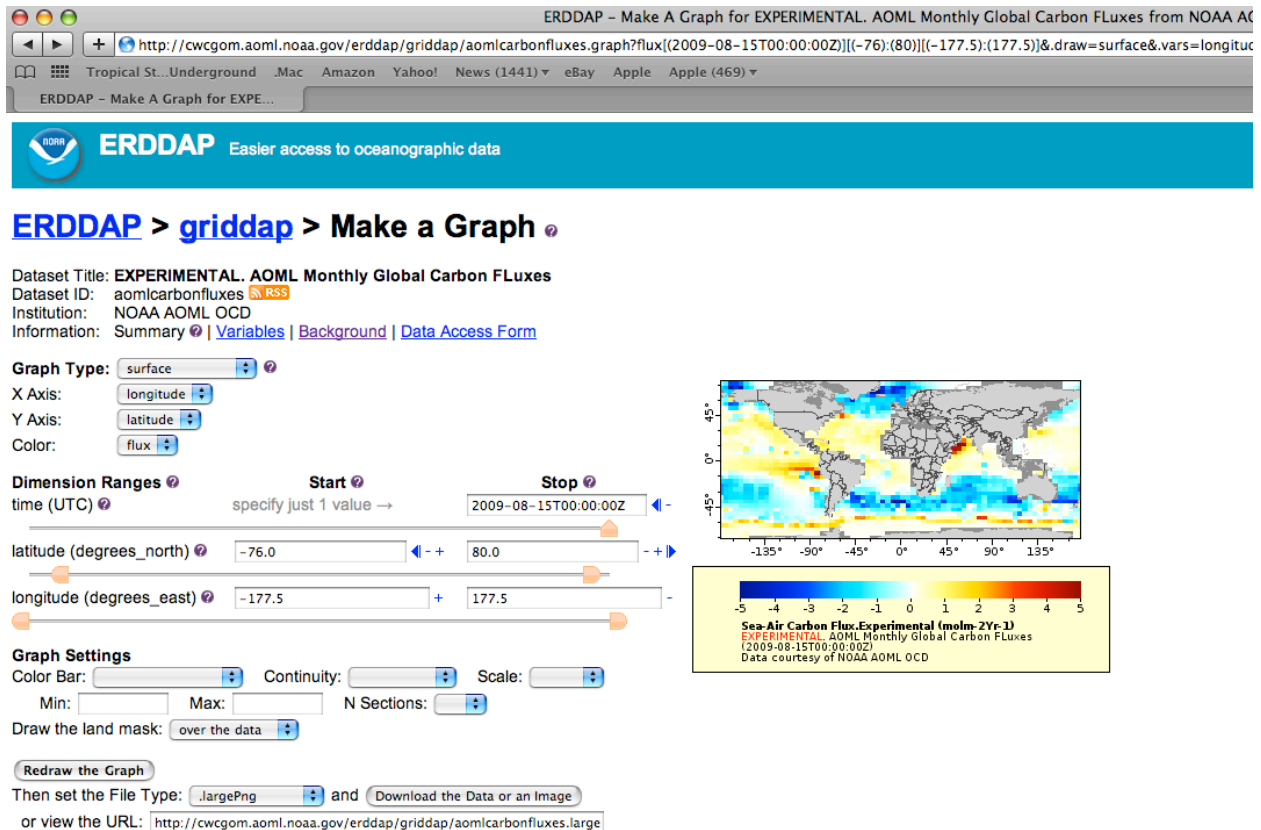


Figure 6. Interface from the web site (<http://cwcgom.aoml.noaa.gov/erddap/griddap/aomlcarbonfluxes.graph>) that enables the retrieval of graphic and numeric data for the empirical air-sea CO₂ flux product discussed in this study.

7. Acknowledgments

This work was supported by NOAA’s Global Carbon Cycle Program, which sponsored the development of the new algorithms described in the proposal entitled “Observation-Based Quantification of Seasonal to Interannual Changes in Air-Sea CO₂ Fluxes” (GC07-193). Funds for managing the CO₂ flux product are provided by NOAA’s Climate Observation Division under the Global Carbon Data Management and Synthesis Project. The program managers, Mike Johnson, Joel Levy, Ken Mooney, and Kathy Tedesco, are gratefully acknowledged for their support. This research was also carried out in part under the auspices of the Cooperative Institute for Marine and Atmospheric Studies (CIMAS), a Joint Institute of the University of Miami and NOAA (cooperative agreement NA17RJ1226).

8. References

- Feely, R.A., T. Takahashi, R. Wanninkhof, M.J. McPhaden, C.E. Cosca, S.C. Sutherland, and M.-E. Carr (2006): Decadal variability of the air-sea CO₂ fluxes in the equatorial Pacific Ocean. *J. Geophys. Res.*, 111, C08S90, doi:10.1029/2005JC003129.
- GLOBALVIEW-CO₂ (2008): Cooperative Atmospheric Data Integration Project-Carbon Dioxide. CD-ROM, NOAA-ESRL, Boulder, Colorado (also available on the Internet via anonymous FTP to ftp.cmdl.noaa.gov, Path: ccg/co2/GLOBALVIEW).
- Kanamitsu, M., W. Ebisuzaki, J. Woollen, S.-K. Yang, J.J. Hnilo, M. Fiorino, and G.L. Potter (2002): NCEP-DOE AMIP-II reanalysis (R-2). *Bull. Amer. Meteorol. Soc.*, 83, 1631-1643.
- Lee, K., R. Wanninkhof, T. Takahashi, S.C. Doney, and R.A. Feely (1998): Low interannual variability in recent oceanic uptake of atmospheric carbon dioxide. *Nature*, 396, 155-159.
- Park, G.-H., K. Lee, R. Wanninkhof, and R.A. Feely (2006): Empirical temperature-based estimates of variability in the oceanic uptake of CO₂ over the past 2 decades. *J. Geophys. Res.*, 111, C07S07, doi:10.1029/2005JC003090.
- Reynolds, R.W., N.A. Rayner, T.M. Smith, D.C. Stokes, and W. Wang (2002): An improved in situ and satellite SST analysis for climate. *J. Climate*, 15, 1609-1625.
- Sabine, C.L., R.A. Feely, N. Gruber, R.M. Key, K. Lee, J.L. Bullister, R. Wanninkhof, C.S. Wong, D.W.R. Wallace, B. Tilbrook, F.J. Millero, T.-H. Peng, A. Kozyr, T. Ono, and A.F. Rios (2004): The oceanic sink for anthropogenic CO₂. *Science*, 305, 367-371.
- Sweeney, C., E. Gloor, A.R. Jacobson, R.M. Key, G. McKinley, J.L. Sarmiento, and R. Wanninkhof (2007): Constraining global air-sea gas exchange for CO₂ with recent bomb ¹⁴C measurements. *Global Biogeochem. Cycles*, 21, GB2015, doi:10.1029/2006GB002784.
- Takahashi, T., W.S. Broecker, S.R. Werner, and A.E. Bainbridge (1980): Carbonate chemistry of the surface waters of the world oceans. In *Isotope Marine Chemistry*, E.D. Goldberg, Y. Horibe, and K. Saruhashi (eds.). Uchida Rokakuho, Tokyo, 291-326.
- Takahashi, T., J. Olafsson, J.G. Goddard, D.W. Chipman, and S.C. Sutherland (1993): Seasonal variation of CO₂ and nutrients in the high-latitude surface oceans: A comparative study. *Global Biogeochem. Cycles*, 7, 843-878.
- Takahashi, T., S. Sutherland, C. Sweeney, A. Poisson, N. Metzl, B. Tilbrook, N. Bates, R. Wanninkhof, R. Feely, and C. Sabine (2002): Global sea-air CO₂ flux based on climatological surface ocean pCO₂ and seasonal biological and temperature effects. *Deep-Sea Res., Part II*, 49, 1601-1622.
- Takahashi, T., S.C. Sutherland, R. Wanninkhof, C. Sweeney, R.A. Feely, D.W. Chipman, B. Hales, G. Friederich, F. Chavez, C. Sabine, A. Watson, D.C.E. Bakker, U. Schuster, N. Metzl, H. Yoshikawa-Inoue, M. Ishii, T. Midorikawa, Y. Nojiri, A. Körtzinger, T. Steinhoff, M. Hoppema, J. Olafsson, T.S. Arnarson, B. Tilbrook, T. Johannessen, A. Olsen, R. Bellerby, C.S. Wong, B. Delille, N.R. Bates, and H.J.W. de Baar (2009): Climatological mean and decadal change in surface ocean pCO₂, and net sea-air CO₂ flux over the global oceans. *Deep-Sea Res., Part II*, 56, 554-577.

- Telszewski, M., A. Chazottes, U. Schuster, A.J. Watson, C. Moulin, D.C.E. Bakker, M. González-Dávila, T. Johannessen, A. Körtzinger, H. Lüger, A. Olsen, A. Omar, X.A. Padin, A.F. Ríos, T. Steinhoff, M. Santana-Casiano, D.W.R. Wallace, and R. Wanninkhof (2009): Estimating the monthly pCO₂ distribution in the North Atlantic using a self-organizing neural network. *Biogeosci.*, 6, 1405-1421.
- Trenberth, K.E. (1997): The definition of El Niño. *Bull. Amer. Meteorol. Soc.*, 78, 2771-2777.
- Wallcraft, A.J., A.B. Kara, C.N. Barron, E.J. Metzger, R.L. Pauley, and M.A. Bourassa (2009): Comparisons of monthly mean 10 m wind speeds from satellites and NWP products over the global ocean. *J. Geophys. Res.*, 114, D16109, doi:10.1029/2008JD011696.
- Wanninkhof, R. (1992): Relationship between wind speed and gas exchange over the Ocean. *J. Geophys. Res.*, 97, 7373-7382.
- Weiss, R.F. (1974): Carbon dioxide in water and seawater: The solubility of a non-ideal gas. *Mar. Chem.*, 2, 203-215.